

Initial Condition Sensitivity of Global Quantities in Magnetohydrodynamic Turbulence

Gaurav Dar*, Mahendra K. Verma

Department of Physics

V. Eswaran

Department of Mechanical Engineering

Indian Institute of Technology, Kanpur 208016, India

November 15, 2018

Abstract

In this paper we study the effect of subtle changes in initial conditions on the evolution of global quantities in two-dimensional Magnetohydrodynamic (MHD) turbulence. We find that a change in the initial phases of complex Fourier modes of the Elsässer variables, while keeping the initial values of total energy, cross helicity and Alfvén ratio unchanged, has a significant effect on the evolution of cross helicity. On the contrary, the total energy and Alfvén ratio are insensitive to the initial phases. Our simulations are based on direct numerical simulation using the pseudo-spectral method.

PACS Number(s): 47.65.+a,47.27.Gs,47.27.Jv

*e-mail: gdar@iitk.ernet.in

In fluid turbulence, the evolution of the velocity, $\mathbf{u}(\mathbf{x})$, at a given position or of a given Fourier component, $\mathbf{u}(\mathbf{k})$, is known to be sensitive to the details of the initial conditions, e.g. phases of $\mathbf{u}(\mathbf{k})$ (to be defined rigorously later). However, the evolution of global quantities like total energy are generally presumed to depend only on initial values of total energy and energy spectrum. The averaging over many modes appear to wash out the effects of the initial phases after a reasonably long time. The total energy in simulations with the same initial energy and spectrum, but with the modes chosen randomly, evolve along nearby trajectories; This is demonstrated in Fig. 1. It has been a common belief that in MHD turbulence also the evolution of global quantities, e.g. total energy and cross helicity, depends only on the initial values of global quantities and their spectra. The evolution of global quantities have earlier been studied by Ting et al. [1], Matthaeus et al. [2, 3], Biskamp and Welter [4], Pouquet et al. [5] in which they found dynamic alignment and various other phenomena. In this paper we show numerically that under certain conditions in two-dimensional (2D) magnetohydrodynamic (MHD) turbulence, the evolution of global quantities may not depend solely only on their initial values, but may depend significantly on more subtle features like the phases of complex Fourier modes (to be defined below) of the initially prescribed fields of the dynamical variables. In other words, a knowledge of the gross initial features as specified by the global quantities is not sufficient under all conditions to determine the evolution of global quantities. We only choose phases as a convenient way of demonstrating the inadequacy of specifying the initial global quantities and spectra alone for computing the evolution of certain global quantities. We find that the evolution of cross helicity shows a sensitivity to the initial phases in simulations with small values of initial cross helicity.

The primary variables in MHD turbulence are the velocity field \mathbf{u} and the magnetic field \mathbf{b} . In our simulations we take mean magnetic field to be zero. We use Elsässer variables

$\mathbf{z}^\pm = \mathbf{u} \pm \mathbf{b}$ in our simulations. These variables denote fluctuations with 'positive' and 'negative' velocity-magnetic field correlations. The relevant quadratic quantities are

$$E^+ = \frac{1}{2} \int_{unit\ vol.} (\mathbf{z}^+)^2 d\mathbf{v} = \frac{1}{2} \sum_{\mathbf{k}} \left(|\mathbf{z}^+(\mathbf{k})|^2 \right), \quad (1)$$

$$E^- = \frac{1}{2} \int_{unit\ vol.} (\mathbf{z}^-)^2 d\mathbf{v} = \frac{1}{2} \sum_{\mathbf{k}} \left(|\mathbf{z}^-(\mathbf{k})|^2 \right), \quad (2)$$

the magnetic energy,

$$\begin{aligned} E_b &= \frac{1}{2} \int_{unit\ vol.} \mathbf{b}^2 d\mathbf{v} \\ &= \frac{1}{8} \sum_{\mathbf{k}} \left(|\mathbf{z}^+(\mathbf{k})|^2 + |\mathbf{z}^-(\mathbf{k})|^2 - 2Re \left(\mathbf{z}^+(\mathbf{k}) \cdot \tilde{\mathbf{z}}^-(\mathbf{k}) \right) \right), \end{aligned} \quad (3)$$

the fluid energy,

$$\begin{aligned} E_u &= \frac{1}{2} \int_{unit\ vol.} \mathbf{u}^2 d\mathbf{v} \\ &= \frac{1}{8} \sum_{\mathbf{k}} \left(|\mathbf{z}^+(\mathbf{k})|^2 + |\mathbf{z}^-(\mathbf{k})|^2 + 2Re \left(\mathbf{z}^+(\mathbf{k}) \cdot \tilde{\mathbf{z}}^-(\mathbf{k}) \right) \right). \end{aligned} \quad (4)$$

and the mean square magnetic vector potential

$$\begin{aligned} A &= \sum_{\mathbf{k}} |\psi(\mathbf{k})|^2 \\ &= \sum_{\mathbf{k}} \frac{|\mathbf{b}(\mathbf{k})|^2}{k^2} \end{aligned} \quad (5)$$

where ψ is the magnetic vector potential, $\tilde{\mathbf{z}}^+$ and $\tilde{\mathbf{z}}^-$ are complex conjugates of \mathbf{z}^+ and \mathbf{z}^- respectively. The total energy is $E = (E^+ + E^-)/2$ and the cross helicity is $H_c = (E^+ - E^-)/2$. There are two well known dimensionless parameters: the normalised cross helicity $\sigma_c = H_c/E$ and the Alfvén ratio $r_A = E_u/E_b$. The total energy, cross helicity, and the mean square vector potential are the three global inviscid invariants of the 2D MHD equation.

We denote the complex Fourier modes $\mathbf{z}^\pm(\mathbf{k})$ by $|\mathbf{z}^\pm(\mathbf{k})| \exp(i\theta_{\mathbf{k}}^\pm)$, where $\theta_{\mathbf{k}}^\pm$ are the phases of the modes. All the three global inviscid invariants E , H_c , and A are independent of phases, while the Alfvén ratio r_A depends on the phase difference $\theta_{\mathbf{k}}^+ - \theta_{\mathbf{k}}^-$. Ting et al. [1] found that the Alfvén ratio affects the evolution of global quantities; it follows from their observations that the initial phase difference $\theta_{\mathbf{k}}^+ - \theta_{\mathbf{k}}^-$ would affect the global evolution. In this paper we demonstrate numerically that even keeping this initial phase difference fixed, change of absolute value of the initial phases $\theta_{\mathbf{k}}^+$ affects the global evolution.

In our simulations we investigate the effects of the initial phases on the subsequent total energy E , normalised cross helicity σ_c , and Alfvén ratio r_A . The temporal evolution of σ_c has been the subject of investigation in a number of earlier studies [1, 2, 3, 4, 5]. In several of these studies, σ_c has been observed to increase with time [2, 3, 4, 5], a behaviour termed as dynamic alignment. However, Biskamp and Welter[4] observed in their simulations that the tendency towards dynamic alignment decreases with the increase in Reynolds number, and σ_c could even decrease at high enough Reynolds number [4]. Ting et al. [1] too observed a few cases of decreasing σ_c for small values of initial σ_c and E/A . In these earlier studies the effects of absolute phases have not been studied.

We solve the 2-D incompressible MHD equations with hyperviscosity. The equations written in terms of the Elsässer variables, \mathbf{z}^+ and \mathbf{z}^- are

$$\begin{aligned} \frac{\partial \mathbf{z}^\pm}{\partial t} \mp (\mathbf{B}_0 \cdot \nabla) \mathbf{z}^\pm + (\mathbf{z}^\mp \cdot \nabla) \mathbf{z}^\pm &= -\nabla p + \nu_\pm \nabla^2 \mathbf{z}^\pm + \nu_\mp \nabla^2 \mathbf{z}^\mp \\ &+ \left(\nu_\pm/k_{eq}^2\right) \nabla^4 \mathbf{z}^\pm + \left(\nu_\mp/k_{eq}^2\right) \nabla^4 \mathbf{z}^\mp \end{aligned} \quad (6)$$

where ν_+ and ν_- are related to the fluid viscosity (ν) and magnetic diffusivity (μ) by the relationship $\nu^\pm = 1/2(\nu \pm \mu)$. The last two terms in Eq. (6) include hyperviscosity ν^\pm/k_{eq}^2

to damp out the energy at very high wave numbers. We choose $\nu = \mu = 5 \times 10^{-4}$ for runs on a grid of size 512×512 and $\nu = \mu = 10^{-3}$ for runs on a grid of size 256×256 . The hyperviscosity related parameter k_{eq} is chosen to be 20 for runs on both the grids. The time step dt used for these runs is 10^{-3} . The simulations are carried up to the final time $t_{\text{final}} = 50$.

We use the pseudo-spectral method [6, 7, 8] to solve the above equations in a periodic box of size $2\pi \times 2\pi$. In order to remove the aliasing errors arising in the pseudo-spectral method a square truncation is performed wherein all modes with $|k_x| \geq N/3$ or $|k_y| \geq N/3$ are set equal to zero. The equations are time advanced using the second order Adam-Bashforth scheme for the convective terms and Crank-Nicholson for the viscous terms. In order to validate our code we used a simulation result of Pouquet et al. [5] for comparison (see Fig. 2).

The simulations are performed for various initial sets of σ_c and r_A values. The initial conditions are generated by first fixing r_A , σ_c , E^+ , and E^- . The chosen value of r_A determines the phase difference $\theta_{\mathbf{k}}^+ - \theta_{\mathbf{k}}^-$. The initial E and σ_c determine $|\mathbf{z}^\pm(\mathbf{k})|$. Note that the absolute phase $\theta_{\mathbf{k}}^+$ is still a free parameter. Only modes within the annular region $1/2 \leq |\mathbf{k}| < 3/2$ are non-zero and each of the modes within this region receives equal energy (i.e., $|\mathbf{z}^\pm(\mathbf{k})|^2 = E^\pm/M$, where M is the number of modes in the shell). The initial states are generated thus for only half the modes - the remaining half are conjugate to them.

The phase sensitivity of the evolution of σ_c , E , and r_A are studied by comparison of pairs of simulations in which initial $\theta_{\mathbf{k}}^+$ are different. We change the initial phases in two ways. In one case we change $\theta_{\mathbf{k}}^+$ uniformly for all the modes by an amount Δ , while in the other case the phases are changed by using a different random seed in the random number generator.

The initial global quantities E , H_c , r_A , and their spectra remain unchanged under these phase changes. The evolution of σ_c for a variety of initial σ_c , r_A and Δ values are shown in Table 1 (pairs of simulations are shown together; for example, mhd1 differs from mhd1* only in that its initial $\mathbf{z}^\pm(\mathbf{k})$ fields have to be shifted from the latter's by $\Delta = 0.4$).

The $N = 512$ runs with $t_{final} = 50$ are very time intensive. Hence only the small initial σ_c runs, which we found to be sensitive to the phases, were carried out for $N=512$. A large number of runs were performed on $N=64$ to explore a wider range of initial conditions. All these results showed behaviour consistent with the results discussed below which are based on the high resolution runs $N=256$ and 512 .

In our simulations, the small σ_c runs showed the most significant dependence on initial phase $\theta_{\mathbf{k}}^+$. For $\sigma_c = 0.1$ and $r_A = 1.5$, we choose Δ to be 0.0 and 0.4 in mhd1 and mhd1* respectively. It is seen in Fig. 3 that phase shifting has a marked effect on the evolution of σ_c . For $\Delta = 0.0$ (mhd1) σ_c increases from its initial value of 0.1 to its final value of 0.129 , whereas for $\Delta = 0.4$ (mhd1*), σ_c decreases to a final value of 0.06 . The total energy (Fig. 4) and the Alfvén ratio (Fig. 5) do not appear to be affected much by the phase shift. We also compare two simulations (mhd1 and mhd1** in Table 1.) in which the initial phases are generated using different random seeds. For these cases also the effect on the evolution of σ_c (Fig. 3) is significant, but the corresponding effects on the evolution of the total energy (Fig. 4) and r_A (Fig. 5) are not noticeable. We also studied the effects of initial phases for the same initial σ_c , but with a large initial $r_A(5.0)$. The runs mhd2 and mhd2* show the effects of changing Δ , while mhd2 and mhd2** show the effects of different random number generator seeds. The results obtained for this case are similar to the run for initial condition with $r_A = 1.5$. In Fig. 6 it is seen that for initial value of $\Delta = 0.0$ (mhd2), σ_c increases

and for initial $\Delta = 0.3$, σ_c decreases. The effect of changing Δ on the total energy (Fig. 7) and r_A (Fig. 8) is seen to be small. Similar results are obtained if we change the seed of the random number generator (compare mhd2 and mhd2**). Hence, σ_c (Fig. 6) is sensitive to the change in the initial phases whereas the total energy (Fig. 7) and r_A (Fig. 8) are not sensitive. Earlier, Ting et al. [1] had observed a decrease in σ_c for small initial σ_c .

We also perform runs at higher initial values of σ_c (mhd3 and mhd3* in Table 1.). The effect of phase shifting for initial $\sigma_c = 0.5$ and $r_A = 5.0$ is shown in Figures 9,10,11. It is seen in Fig. 9 that the changes in evolution caused by phase shifting are relatively smaller for high initial σ_c values as compared to small initial σ_c discussed above. From Fig. 10 it can be seen that the effect of Δ on total energy is also small and r_A (Fig. 11) remains insensitive to the change in Δ . We have performed more runs than have been shown here and in all cases σ_c was seen to increase for high σ_c values. This increase in σ_c is consistent with simulations performed earlier for high σ_c values [1, 2, 3, 4, 5].

From the numerical results presented here we conclude that phases of the initial modes play an important role in the evolution of σ_c , atleast for cases with small initial σ_c values. For higher values of σ_c , phases do not appear to affect the evolution of σ_c by any significant amount. In all the runs the total energy and r_A were seen not to have any significant dependence on the phases.

The origin of the phase effects discussed here is not clear at this moment. We need to examine the evolution more carefully before reaching any definite conclusion. These studies could find applications in understanding the solar wind observations in which σ_c has been observed to decrease [9, 10, 11, 12].

It has been demonstrated in the paper that the evolution of normalised cross helicity

is significantly affected by subtle features of the initial condition especially at low initial cross helicities. This observation will require us to be more circumspect in drawing conclusions based on arbitrary initial conditions and to exercise more care in choosing the initial conditions in MHD turbulence.

We are thankful to Dr. R. K. Ghosh for providing us computer time through the project TAPTEC/COMPUTER/504 sponsored by All India Council for Technical Education (AICTE). This work was also supported by Department of Science and Technology (DST) India project SR/SY.P-11/94.

References

- [1] A. C. Ting, W. H. Matthaeus, and D. Montgomery. *Phys. Fluids*, 29:9695, 1986.
- [2] W. H. Matthaeus, M. L. Goldstein, and D. C. Montgomery. *Phys. Rev. Lett.*, 51:1484, 1984.
- [3] W. H. Matthaeus and D. Montgomery. in *Statistical Physics and chaos in Fusion Plasmas*, eds. C. W. J. Horton and L. E. Reichl (Wiley, New York), page 285.
- [4] D. Biskamp and H. Welter. *Phys. Fluids B*, 1:1964, 1989.
- [5] A. Pouquet, P. L. Sulem, and M. Meneguzzi. *Phys. Fluids*, 31:2634, 1988.
- [6] S. A. Orszag and G. S. Patterson. *Phys. Rev. Lett.*, 28:76, 1972.
- [7] V. Eswaran and S. B. Pope. *Phys. Fluids*, 31:506, 1988.
- [8] M. K. Verma, D. A. Roberts, M. L. Goldstein, S. Ghosh, and W. T. Stribling. *J. Geophys. Res.*, 101:21619, 1996.
- [9] D. A. Roberts, L. W. Klein, M. L. Goldstein, and W. H. Matthaeus. *J. Geophys. Res.*, 92:11021, 1987a.
- [10] D. A. Roberts, L. W. Klein, M. L. Goldstein, and W. H. Matthaeus. *J. Geophys. Res.*, 92:12023, 1987b.
- [11] E. Marsch and C. Y. Tu. *J. Geophys. Res.*, 95:8211, 1990.
- [12] W. H. Matthaeus and M. L. Goldstein. *J. Geophys. Res.*, 87:6011, 1982a.

FIGURE CAPTIONS

Figure 1. Energy evolution for fluids. The two cases shown here differ only in the phases of the initial conditions. The modes in the runs were $|\mathbf{u}(\mathbf{k})| \exp^{i(\theta_{\mathbf{k}} + \Delta)}$ with $\Delta = 0.0$ and 0.4 .

Figure 2. Time evolution of kinetic (solid line) and magnetic (dashed line) energies for the O-T vortex using a set of parameters from Pouquet et al. (Pouquet et al's results are shown by diamonds and crosses). Here $\nu = 2.5 \times 10^{-3}$ and hyperviscosity is zero.

Figure 3. Normalised cross helicity (σ_c) evolution for initial $\sigma_c = 0.1$, $r_A = 1.5$. The curves shown correspond to mhd1, mhd1*, and mhd1** in Table 1.

Figure 4. Evolution of total energy (E) for same initial conditions as in Fig. 3. See Table 1. for description of mhd1, mhd1*, and mhd1**.

Figure 5. Evolution of Alfvén ratio (r_A) for same initial conditions as in Fig. 3. Look at Table 1. for description of mhd1, mhd1*, and mhd1**.

Figure 6. Normalised cross helicity (σ_c) evolution for initial $\sigma_c = 0.1$, $r_A = 5.0$. The curves shown correspond to mhd2, mhd2*, and mhd2** in Table 1.

Figure 7. Evolution of total energy (E) for same initial conditions as in Fig. 6. Look at Table 1. for description of mhd2, mhd2*, and mhd2**.

Figure 8. Evolution of Alfvén ratio (r_A) for same initial conditions as in Fig. 6. Look at Table 1. for description of mhd2, mhd2*, and mhd2**.

Figure 9. Normalised cross helicity (σ_c) evolution for initial $\sigma_c = 0.5$ and $r_A = 5.0$. The curves shown correspond to mhd3, mhd3* in Table 1.

Figure 10. Evolution of total energy (E) for same initial conditions as in Fig. 9. Look at Table 1. for description of mhd3, mhd3*.

Figure 11. Evolution of Alfvén ratio for same initial conditions as in Fig. 9. Look at Table 1. for description of mhd3, mhd3*.

Table 1: Initial values of the random number generator seed Δ , σ_c and r_A for runs performed on grid of size $N \times N$. The initial and the final values (at $t_{final} = 50$) of σ_c are also shown.

Run	N	Seed	r_A	Δ	$\sigma_c(t=0)$	$\sigma_c(t=50)$	σ_c increases/decreases
mhd1	512	50	1.5	0.	0.1	0.06	decreases
mhd1*	512	50	1.5	0.4	0.1	0.13	increases
mhd1**	512	575	1.5	0.	0.1	0.20	increases
mhd2	512	50	5.0	0.	0.1	0.22	increases
mhd2*	512	50	5.0	0.3	0.1	0.05	decreases
mhd2**	512	575	5.0	0.	0.1	0.13	increases
mhd3	256	50	5.0	0.	0.5	0.87	increases
mhd3*	256	50	5.0	0.4	0.5	0.88	increases
mhd4	64	50	1.5	0.	0.1	0.02	decreases
mhd4*	64	50	1.5	0.6	0.1	0.34	increases
mhd4**	64	50	1.5	1.0	0.1	0.17	increases
mhd5	64	50	2.0	0.	0.1	- 0.02	decreases
mhd5*	64	50	2.0	0.2	0.1	- 0.01	decreases
mhd5**	64	50	2.0	0.4	0.1	0.22	increases
mhd6	64	50	1.0	0.	0.5	0.79	increases
mhd6*	64	50	1.0	0.2	0.5	0.74	increases
mhd6**	64	50	1.0	0.4	0.5	0.72	increases

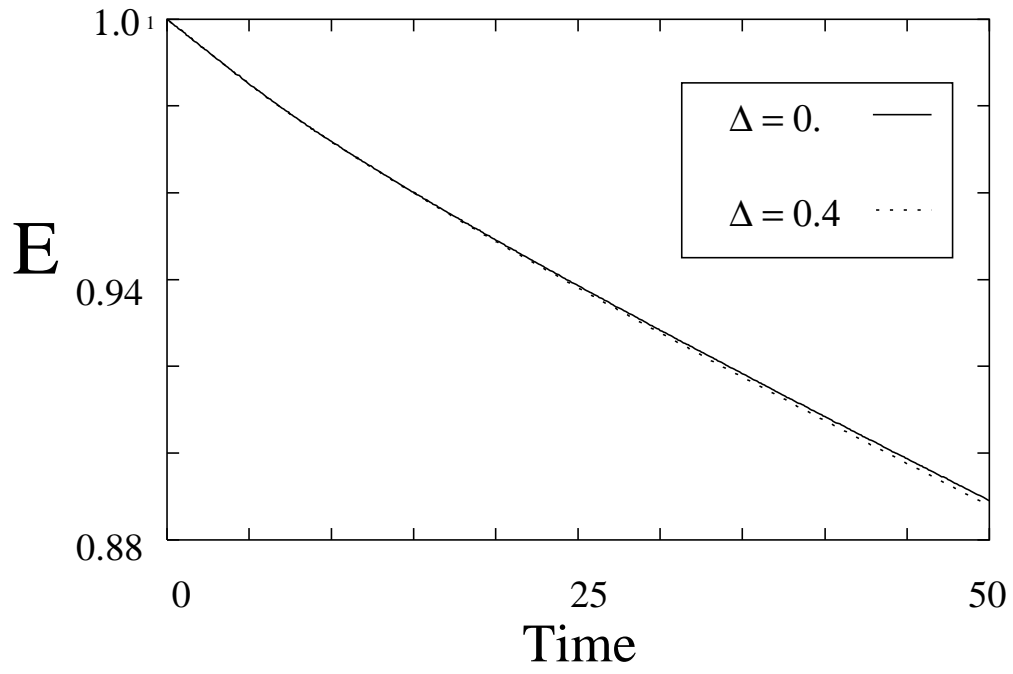


Fig. 1

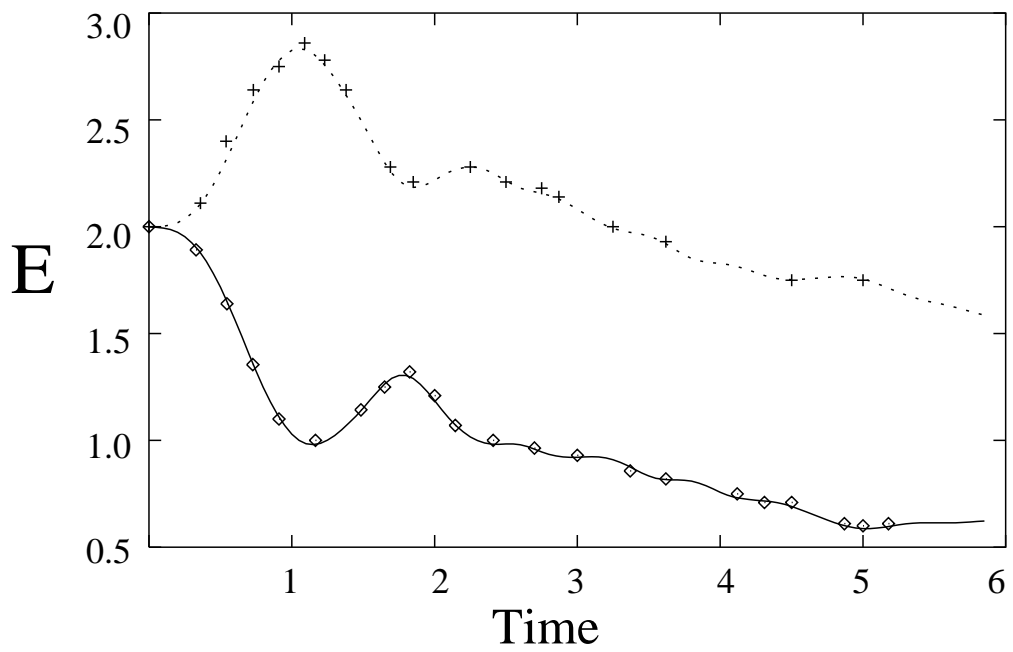


Fig. 2

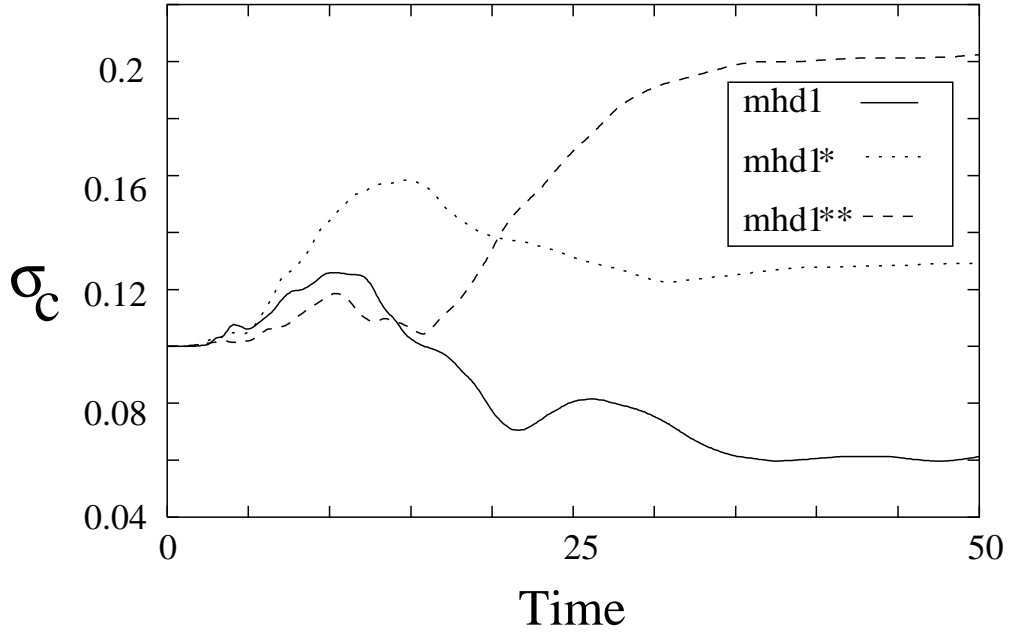


Fig. 3

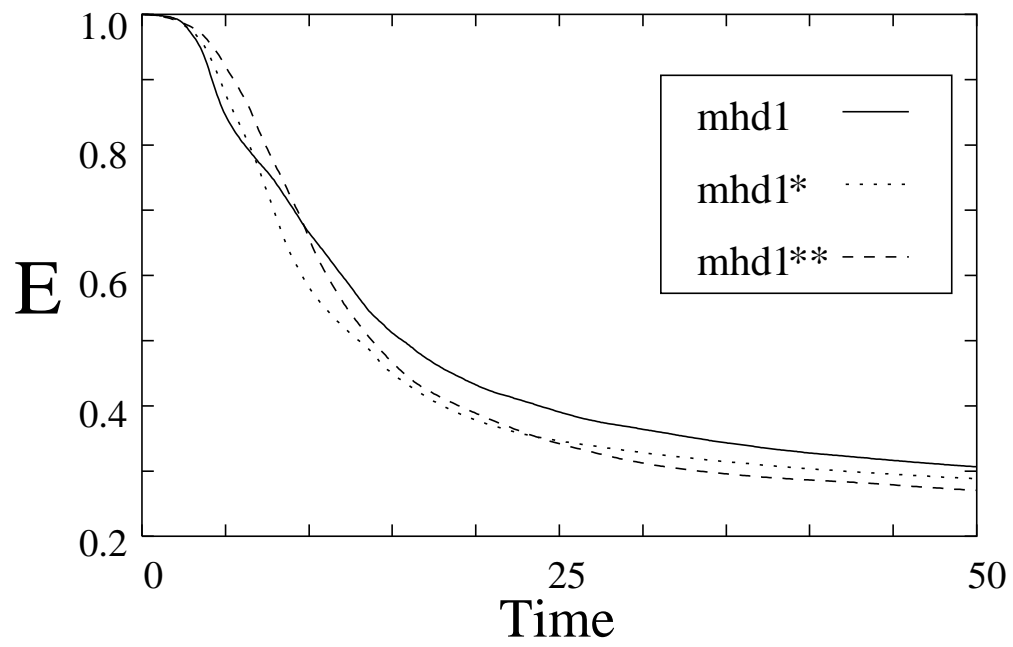


Fig. 4

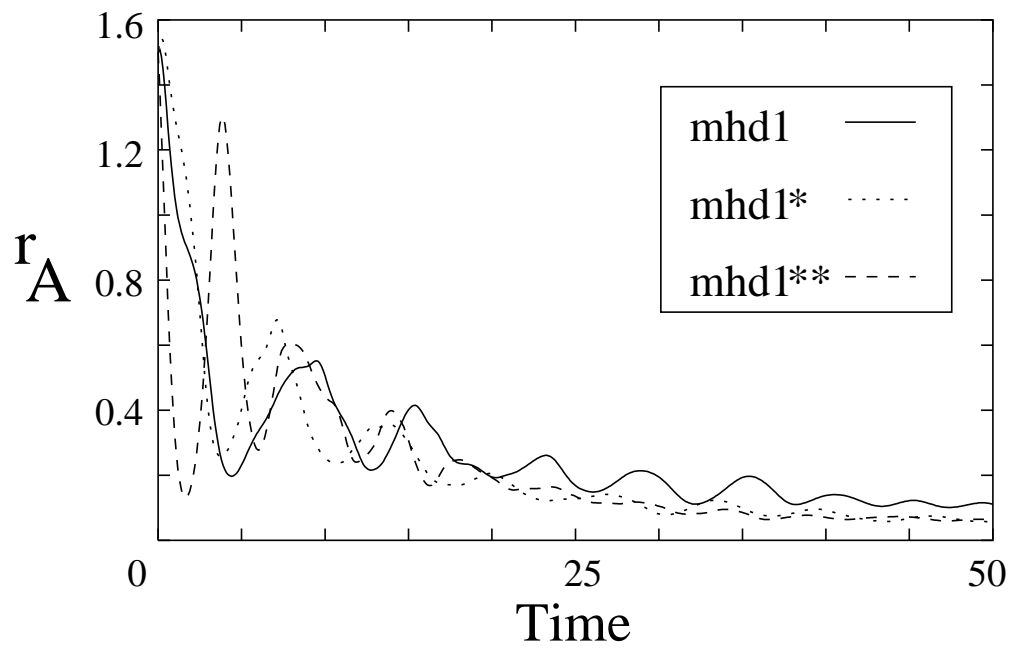


Fig. 5

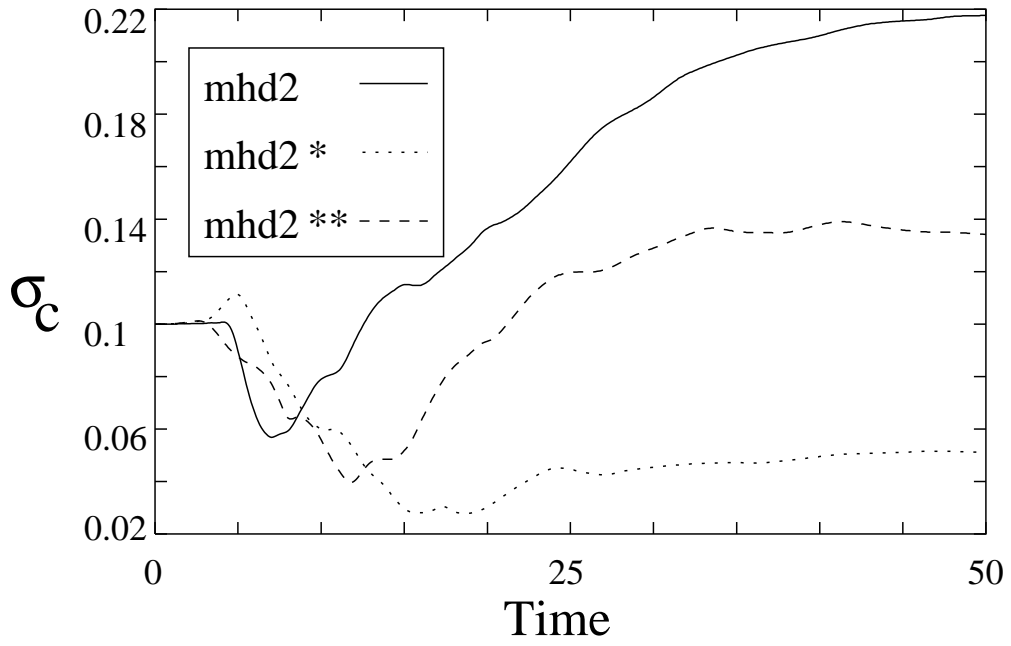


Fig. 6

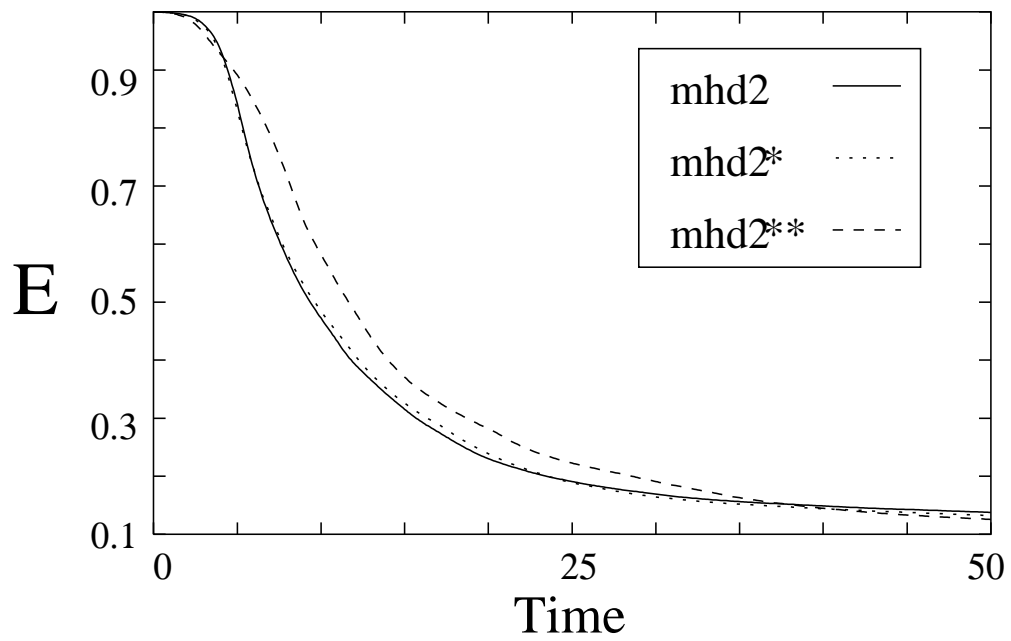


Fig. 7

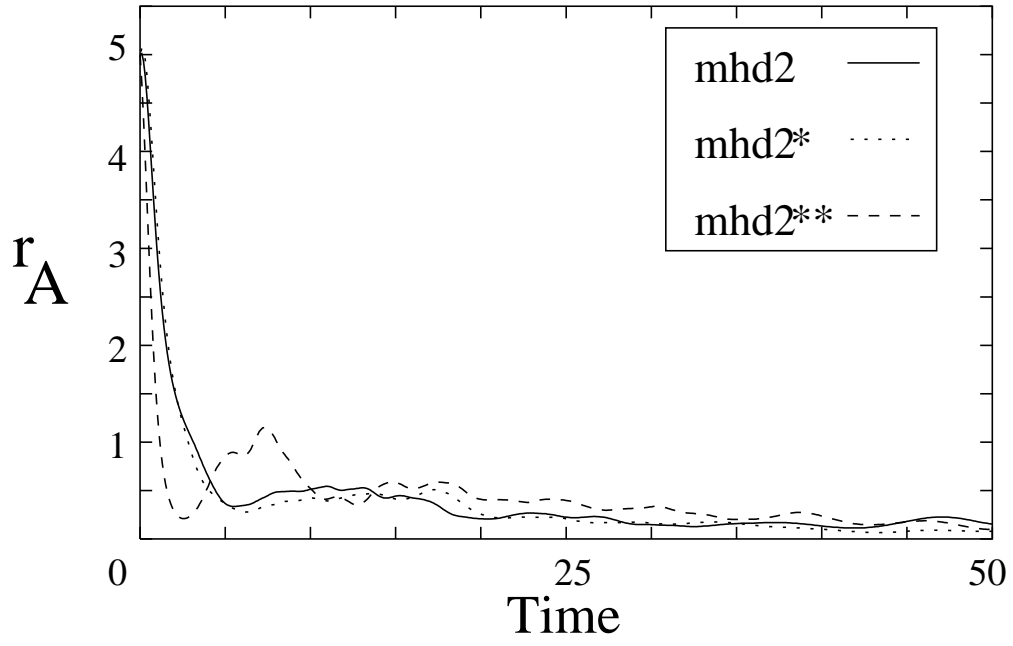


Fig. 8

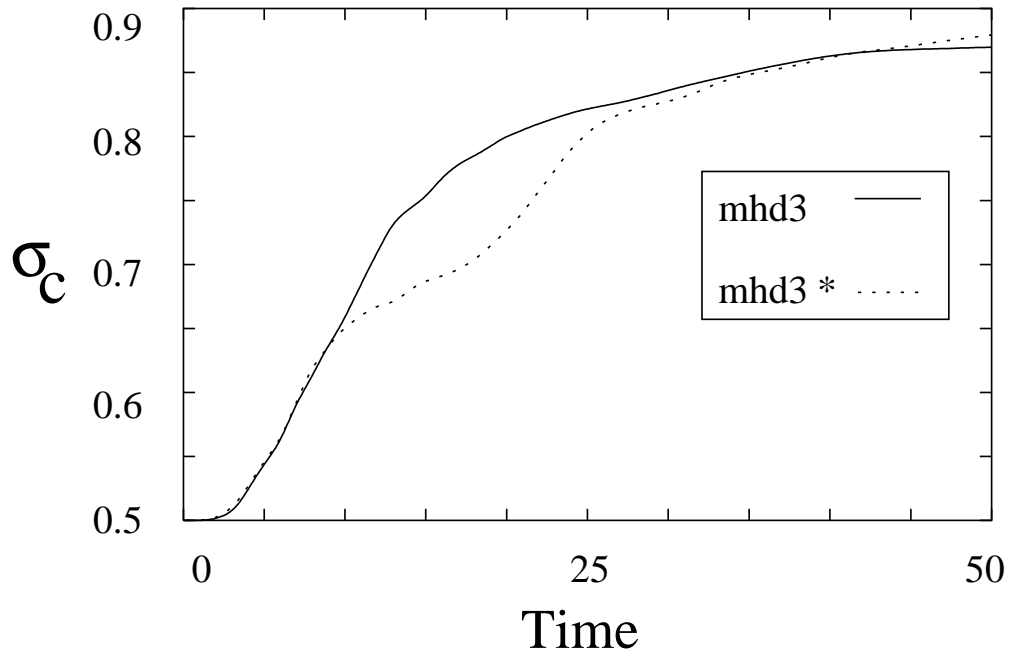


Fig. 9

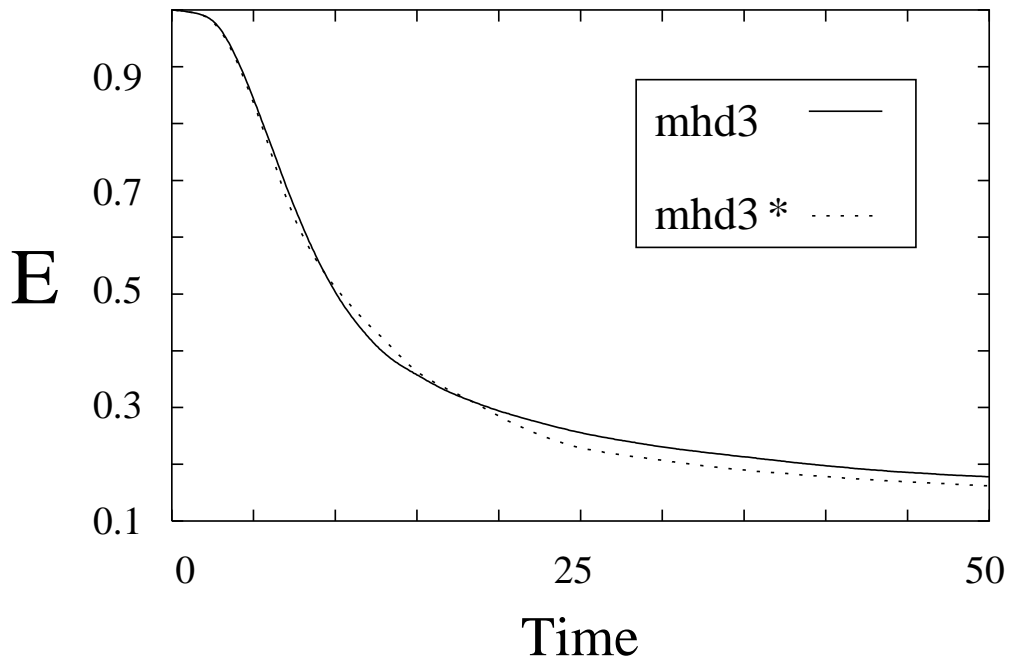


Fig. 10

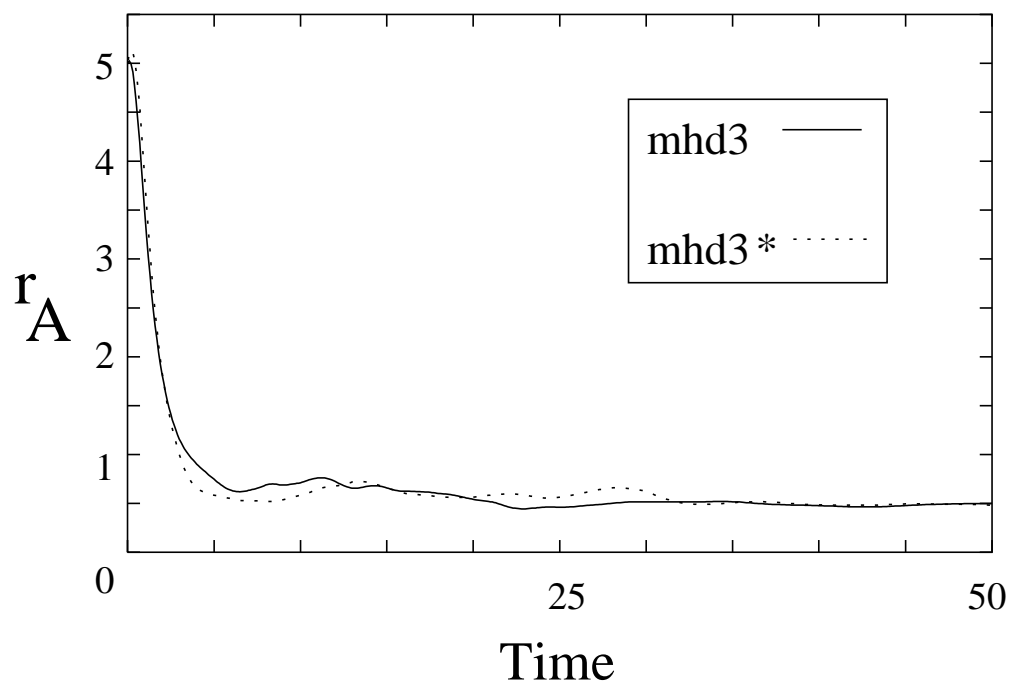


Fig. 11